Multisensor Analysis of a Squall Line in the Amazon Region

Article *in* Journal of Geophysical Research Atmospheres · September 2002

DOI: 10.1029/2000JD000305

CITATIONS
14

READS
83

8 authors, including:

Maria A F Dias
University of São Paulo
292 PUBLICATIONS 10,386 CITATIONS
SEE PROFILE

Rachel I. Albrecht
University of São Paulo
64 PUBLICATIONS 1,279 CITATIONS
SEE PROFILE

Adilson Wagner Gandu
University of São Paulo
59 PUBLICATIONS 584 CITATIONS
SEE PROFILE

Oswaldo Massambani
University of São Paulo
22 PUBLICATIONS 256 CITATIONS
SEE PROFILE

JOURNAL OF GEOPHYSICAL RESEARCH, VOL. 107. NO. D20, 8084, doi:10.1029/2000JD000305, 2002

Multisensor analysis of a squall line in the Amazon Region

Augusto J. Pereira Filho, Maria A. F. Silva Dias, Rachel I. Albrecht, Luis G. P. Pereira, Adilson W. Gandu, and Oswaldo Massambani
Department of Atmospheric Sciences, University of São Paulo, São Paulo, Brazil

Ali Tokay
Tropical Rainfall Measurement Mission Office, NASA Goddard Space Flight Center, Maryland, USA

Steve Rutledge
Department of Atmospheric Sciences, Colorado State University, Colorado, USA

Received 27 December 2000; revised 9 July 2001; accepted 14 August 2001; published 15 October 2002.

[1] Mesoscale features of the 26 January 1999 squall line are described with measurements made during the field experiment in Rondônia, Brazil, in the wet season (WET) of the Amazon region (AMC) as part of the Large-Scale Biosphere-Atmosphere Experiment in the Amazon (LBA) and the Tropical Rainfall Measurement Mission (TRMM); henceforth referred to as the WET AMC and TRMM-LBA field experiment. The squall line moved through the experiment area from northeast to southwest with high rainfall rates in its leading edge and a poorly defined trailing stratiform precipitating area. Polarimetric and Doppler measurements from the Portable Polarimetric S-band Radar (S-POL) were analyzed in conjunction with surface and upper level data, satellite visible (VIS) and infrared (IR) measurements. These remote and local measurements of variables such as cloud spatial and temporal distribution, pressure, temperature, moisture, precipitation, and wind fields are consistent with each other as well as with similar mesoscale dynamics and thermodynamics features measured, analyzed, and modeled elsewhere [e.g., *Rotunno et al.*, 1988; *Garstang et al.*, 1994; *Houze et al.*, 1990]. This tropical squall line is similar to its cousins in the midlatitudes with finer-scale structural and dynamic features such as rotation and divergence. Results suggest that the cold pool has its origins in midlevels between 400 and 600 hPa from where evaporative cooling and drop-dragging bring down colder air to the surface. The convective region is dominated by warm microphysics, while the stratiform region is dominated by cold microphysics. Moreover, both regions are characterized by monomodal drop spectra centered around 2.0 and 1.0 mm, respectively. Horizontal circulation associated with strong updrafts tends to increase cloud growth efficiency in the leading edge of the squall line. *INDEX TERMS:* 3314 Meteorology and Atmospheric Dynamics: Convective processes; 3329 Meteorology and Atmospheric Dynamics: Mesoscale meteorology; 3354 Meteorology and Atmospheric Dynamics: Precipitation (1854); 3360 Meteorology and Atmospheric Dynamics: Remote sensing; 3374 Meteorology and Atmospheric Dynamics: Tropical meteorology; *KEYWORDS:* cloud microphysics, cold pool, squall line, Amazon, remote sensing, mesoscale dynamics

Citation: Pereira Filho, A. J., M. A. F. Silva Dias, R. I. Albrecht, L. G. P. Pereira, A. W. Gandu, O. Massambani, A. Tokay, and S. Rutledge, Multisensor analysis of a squall line in the Amazon Region, *J. Geophys. Res.*, *107*(D20), 8084, doi:10.1029/2000JD000305, 2002.

1. Introduction

[2] Bands of heavy rainfall followed by stratiform precipitation [*Houze et al.*, 1990] are often observed from equatorial regions to midlatitudes. *Browning and Ludlam* [1962] developed one of the first models to explain the airflow within these squall lines. *Houze et al.* [1989] developed a conceptual model based on weather radar measurements to explain the ascending front-to-rear flow and the descending rear inflow within the trailing stratiform region. Numerical simulations by *Fovell and Ogura* [1988, 1989] show important features of squall lines such as the cold air pool, the front-to-rear updraft tilting and the environment vertical wind shear. Doppler weather radar measurements have also been used to analyze (three-dimensional) 3-D airflow and rainfall patterns inside convective systems [*Smull and Houze*, 1987; *Houze et al.*, 1989]. On the other hand, *Biggerstaff and Houze* [1991a, 1991b] proposed a more complete conceptual model for midlevel dynamic and rain-

0148-0227/02/2000JD000305$09.00

fall structures within squall lines based on high-resolution data sets that stresses the impact of the relative horizontal vorticity and the interaction between the convective leading edge and the trailing stratiform region. Furthermore, *Braun and Houze* [1994] analyzed the microphysics and the thermodynamics of squall lines to explain the secondary rainfall maximum in the stratiform region. Mesoscale surface measurements by *Johnson and Hamilton* [1988] also indicate a relationship between surface low- and high-pressure systems and rainfall patterns around squall lines.

[3] Squall lines are among a myriad of convective systems in Brazil [*Silva Dias*, 1999]. Several squall lines have been studied in different regions of Brazil. These studies have been based on limited surface, upper air, radar and satellite measurements to characterize their internal structure, their time evolution [*Gandú*, 1984; *Lima*, 1985; *Pereira Filho et al.*, 1991; *Beneti*, 1991; *Gomes et al.*, 1996], and their associated synoptic environment [*Scolar*, 1983]. Doppler radar measurements have also been used to classify squall lines [*Abdoulaev and Lenskaia*, 1996a], to characterize their evolution, motion [*Abdoulaev and Lenskaia*, 1996b], internal kinetic structure [*Abdoulaev and Lenskaia*, 1996c], and wind gusts [*Lenskaia and Abdoulaev*, 1996]. The life cycle of squall lines were also studied through satellite measurements [*Machado et al.*, 1994]. Several other analysis of convective systems and their climatology over South America includes reports by *Negri et al.* [2000], *Silva Dias* [1999, 1989], *Garreaud and Wallace* [1997, 1998], *Hastenrath* [1997], *Gash et al.* [1996], *Cohen et al.* [1995], *Garstang et al.* [1994], and *Greco et al.* [1994]. In the recent past, due to a lack of observations, numerical simulations have been used to study squall lines over the Amazon region [*Silva Dias and Ferreira*, 1992; *Ambrizzi*, 1989]. Recently, a large set of observations were produced by the WET AMC TRMM-LBA henceforth TRMM-LBA, Brazil [*Silva Dias*, 2002]. The LBA studies are providing a greater inside into the dynamics, thermodynamics and microphysics of squall lines over equatorial regions.

[4] One of the goals of the WET/AMC TRMM-LBA project in Rondônia, Brazil [*Silva Dias*, 2002], carried out between January and February 1999, was to study the spatial and temporal evolution of convective systems in the Amazon region. In this manuscript, the 26 January 1999 squall line that passed over the TRMM-LBA experiment area is analyzed. This mesoscale system can be seen in the GOES-8 enhanced IR images between 1945 and 2245 UTC (Figure 1). The squall line moved from northwest to southeast at 12 m s^{-1}. Colder cloud tops are associated with the leading edge of the convective band while less cold cloud tops are observed in the rear side stratiform region. This squall line resembles those documented and analyzed by *Houze et al.* [1989] and by *Brawn and Houze* [1994] in Northern Hemisphere midlatitudes.

[5] The objectives of this work are: (1) to describe mesoscale features (e.g., vertical and horizontal dimensions, low-level convergence, upper level divergence, the cold air pool and the low-level jet), cloud-scale features (e.g., 3-D structure of convective and stratiform clouds, turbulence, updrafts and downdrafts) and microphysical characteristics (e.g., convective and stratiform rainfall, hydrometer types and drop spectra) with high-resolution surface, upper air and weather radar measurements; and (2) to analyze the microphysical, dynamic and thermodynamic structures of this tropical squall line [*Garstang et al.*, 1994].

2. Methodology

[6] Figure 2 shows the TRMM-LBA experiment area and measurement sites. The array of instruments include automatic weather stations, rain gauges, disdrometers, lightning sensors, tethered balloons, radiosonde, weather radars, the TRMM satellite, the GOES-8 east satellite, aircrafts, among other air quality sensors. The 1800 and 2100 UTC radiosonde at Rolim de Moura (Figure 2) on 26 January 1999 are used in this work to study the thermodynamic structure of the atmosphere before and during the passage of the squall line over that site.

[7] Surface measurements of temperature (°C), relative humidity (%), wind speed (m s^{-1}) and direction (degree), pressure (hPa) and rainfall accumulation (mm) at Rolim the Moura were used to analyzed the cold pool intensity, mesoscale pressure features and their respective circulation. Microphysical features were measured and analyzed with the disdrometer [*Tokay et al.*, 1999] and the vertical-pointing S-Band radar [*Ecklund et al.*, 1999] at the Ji-Paraná airport (Figure 2). This S-band radar measures reflectivity, velocity and spectral width with high temporal resolution at 105 m intervals in the vertical.

[8] The squall line dynamics and microphysics were also analyzed with horizontal and vertical cross sections obtained with the S-POL weather radar data [*Lutz et al.*, 1995]. It is an S-Band polarized Doppler radar with a peak transmitting power of 1.2 MW, 1.0° half power beam width, 1 μs pulse width and a dynamic pulse repetition frequency between 325 and 1200 Hz. The S-POL weather radar measures nine polarimetric, phase and power variables. This work utilizes the horizontal reflectivity or Z_h ($mm^6 m^{-3}$), the differential reflectivity or Z_{DR} (dB), the linear polarization or LDR, the Doppler radial velocity or VE (m s^{-1}) and spectral width or SW (m s^{-1}). The horizontal reflectivity is a volumetric measurement of the drop spectrum to the six power and is related to the rainfall rate or R (mm h^{-1}) by a theoretical Z-R relationship. The reflectivity is transformed to logarithmic scale due to its wide range of values. For instance, fair weather cumulus measures −15 dBZ while heavy rainfall or hail measures around 60 dBZ. The linear polarization is useful to identify hydrometeor types. Raindrops and snow yield between −35 and −15 dB while elongated ice crystals give positive values. The differential reflectivity can be used to estimate rainfall rates and to detect hail. Perfectly round spheres yield 0 dB while large oblate drops up to 5 dB. The radial velocity measures movement toward (negative) and away (positive) from the radar. The spectral width is a measure of radial speed variance and is in general related to turbulence. Further information on polarimetric measurements are given by *Zrnic and Ryzhkov* [1999].

3. Results

3.1. S-POL Measurements

[9] Fields of reflectivity, differential reflectivity, radial winds and linear polarization in a 0.7° plan position indicator

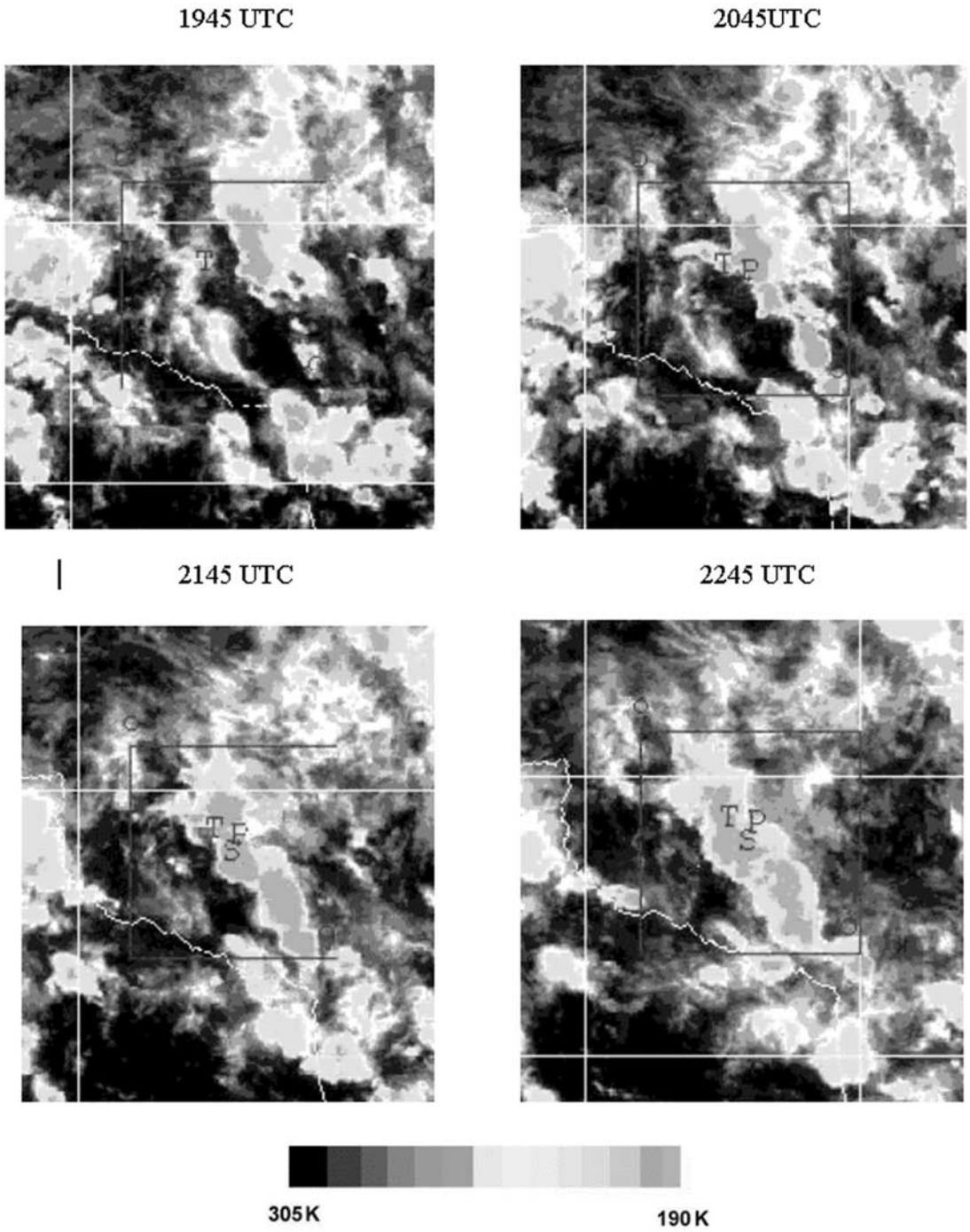

Figure 1. GOES-8 enhanced IR images on 26 January 1999. The inner square indicates the WET/AMC TRMM-LBA experiment area. Letters indicate the location of the S-POL weather radar (S), the TOGA weather radar (T), and the vertical-pointing weather radar in Rondônia. White lines indicate geographic contours and latitudes and longitudes. Colorscale indicates estimated temperatures (K). The latitudes and longitudes of the inner rectangle are approximately −9°S, −13°S, −64°W, and −60°W.

(PPI) at 2015 UTC, 26 January 1999 are shown in Figure 3. The radial wind field in Figure 3a shows mesoscale features such as a low-level jet (descending rear inflow) near the leading edge at about 60° azimuth and 50 to 75 km range with wind speeds greater than 18 m s^{-1} toward the radar, an area of cyclonic convergence on the left flank at 30° azimuth and 80 km range, and an area of convergence within a convective cell to the west of the squall line nearly 315° azimuth at 90 km range. The clear echo region between the radar and the squall line indicate outbound winds less than 6 m s^{-1} and within the squall line inbound mean winds of 12 m s^{-1}. This average speed agrees well with the satellite estimate and indicates the speed of the cold pool [*Parker*, 1996]. It was generated by cooler air brought down from the

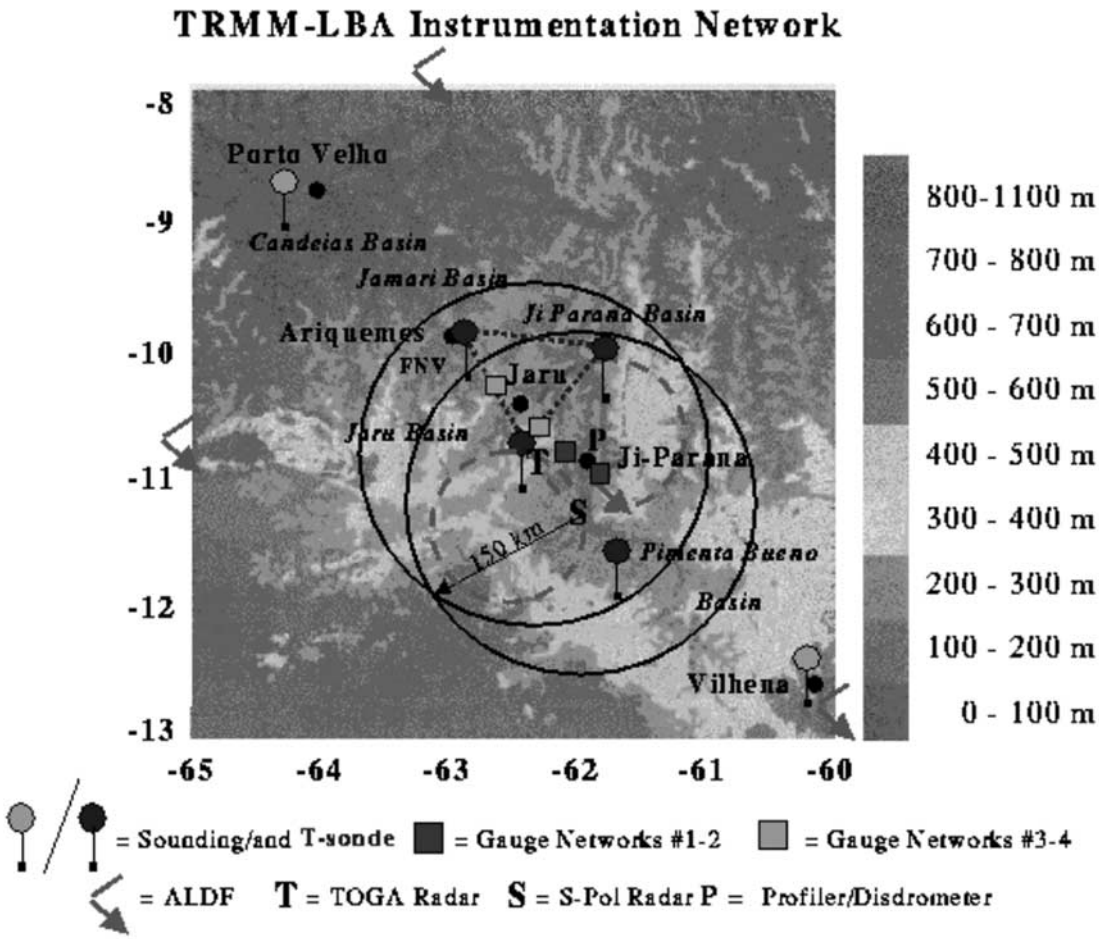

Figure 2. Topographic map of the WET/AMC TRMM-LBA experiment area in Rodônia, Brazil in January and February 1999. Major city locations, sounding sites, surface networks, and weather radars are indicated in the map. The colorscale to the right indicates surface altitudes. It is also indicate the respective longitudes and latitudes at 1° resolution. Circles indicate the TOGA and the S-POL weather radar surveillance limits.

mid levels by rainfall dragging and evaporative cooling caused by mixing with drier environment air [*Johnson*, 2001; *Rotunno et al.*, 1988; *Seitter*, 1986].

[10] The reflectivity field in Figure 3b indicates a band of heavy rainfall with intensities greater than 55 dBZ followed by a larger area of stratiform rainfall with reflectivities around 30 dBZ. This stratiform region is much larger to the northern edge of the system and it resembles the asymmetric stratiform squall archetype described by *Houze et al.* [1990], except that the strongest convective echoes are in that same region. The classification proposed by *Houze et al.* [1990] indicates that there are no preference for the most intense convective cells to be found at any particular location along a symmetric squall line. In the asymmetric case, stronger convective cells are found toward one end of the squall, while weaker, dying cells on the verge of becoming stratiform are found toward the other end of the line. They also found a significant number of mesoscale precipitation systems whose echo patterns bore no apparent resemblance to either of those above. Thus, in the present study, the squall line resembles more a symmetric case of *Houze et al.* [1990].

[11] The convergence area in the radial wind field produced a strong convective cell with reflectivities similar to the ones in the leading edge of the squall line. An almost symmetric area of ground clutter contamination is also apparent out to 20 km range; the radial wind field is not coherent and close to zero.

[12] Differential reflectivities are mostly positive in the field depicted in Figure 3c. Narrow bands of Z_{DR} greater than 3 dB are less than 3 km wide and located at the leading edge of the squall line. Thus one might expect larger raindrops in this region of stronger updrafts and turbulence. Nevertheless, positive values of Z_{DR} indicate a spectrum of fairly oblate raindrops even in the stratiform region near the surface. Comparing both Z and Z_{DR} fields it can be inferred that the respective gradients are larger for the differential reflectivity and also show finer details of the rainfall structure and a clear picture of the drop-size spectrum. The linear polarization field in Figure 3d shows high negative values within the convective and the stratiform regions. Low negative values are observed in the clear air region out to 60 km from the S-POL. The LDR increases rapidly toward the edges of the squall line. These observa-

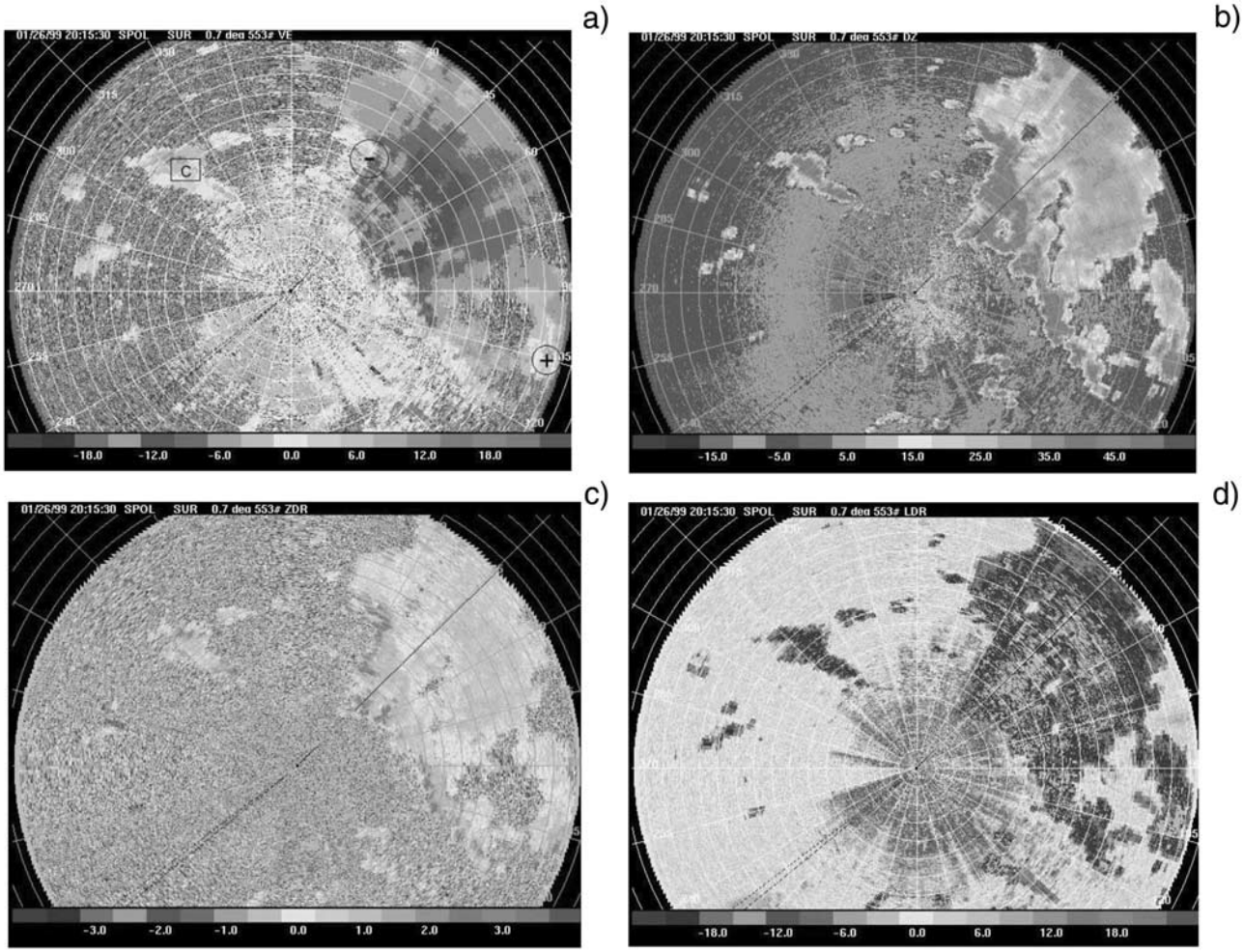

Figure 3. Sector scans of radial wind (a), reflectivity (b), differential reflectivity (c), and linear polarization (d) on a 0.7° plan position indicator measured with the S-POL weather radar at 2015 UTC, 26 January 1999 in Rondônia, Brazil. Colorscale at the bottom of each map are in m s^{-1} (a), dBZ (b), dB (c), and (d). Concentric circles indicate the distance from the radar at 10 km steps and straight lines indicate the azimuth in relationship to the geographic north at 15° steps. In the radial velocity field signs "+," "−," and "c" indicate counterclockwise rotation, clockwise rotation, and convergence signatures, respectively.

tions indicate the dominance of raindrops (high negative LDR) and droplets (low negative LDR) near the surface.

[13] Vertical cross sections of the variables in Figure 3 are shown in Figure 4 for 1958 UTC, 26 January 1999 at 49.0° azimuth. This angle is close to the direction of propagation of the squall line. The radial wind speed in Figure 4a shows a front-to-rear airflow starting at the surface and rapidly ascending between 60 and 80 km and extending downward to the maximum range (150 km). Below this outbound flow, a layer of rear flow extends up to the 65 km range with near-to-surface radial wind speeds of 15 m s^{-1} between 85 and 105 km range. A convergence area near the surface is seen around 75 km range as well as a divergence zone at 10 km height and 80 km range. It indicates tilted updrafts. Another region of strong divergence aloft is in the anvil region with positively tilted inbound speeds of up to 21 m s^{-1}. A region of outbound winds near the surface ahead of the squall line show speeds of less than 3 m s^{-1} while inbound winds within the squall line near the surface and above are much larger. Thus it indicates that most of the shear near the surface is caused by the moving squall line. Qualitatively, horizontal vorticity features depicted in Figure 4a and the reflectivity cross section in Figure 4b suggest that the circulation of the cold pool is almost balanced by both the ambient vertical shear and the vertical shear associated with the rear jet [*Bluestein*, 1993].

[14] Figure 4b shows a family of convective cells from their early stage of development at 47 km range to the decaying phase beyond 90 km range. Mature cells with overshooting tops are in between 70 and 80 km, where the strongest convergence (below) and divergence (aloft) are located. New cells form underneath the anvil between 40 and 55 km, where there is intense counterclockwise horizontal vorticity produced by the updraft ahead of the squall. High rainfall rates are in general below 5 km height with peaks above 55 dBZ in the convective region and around 35 dBZ in the stratiform region. The bright band is not evident in Figure 4b due to intense turbulent mixing in the convective

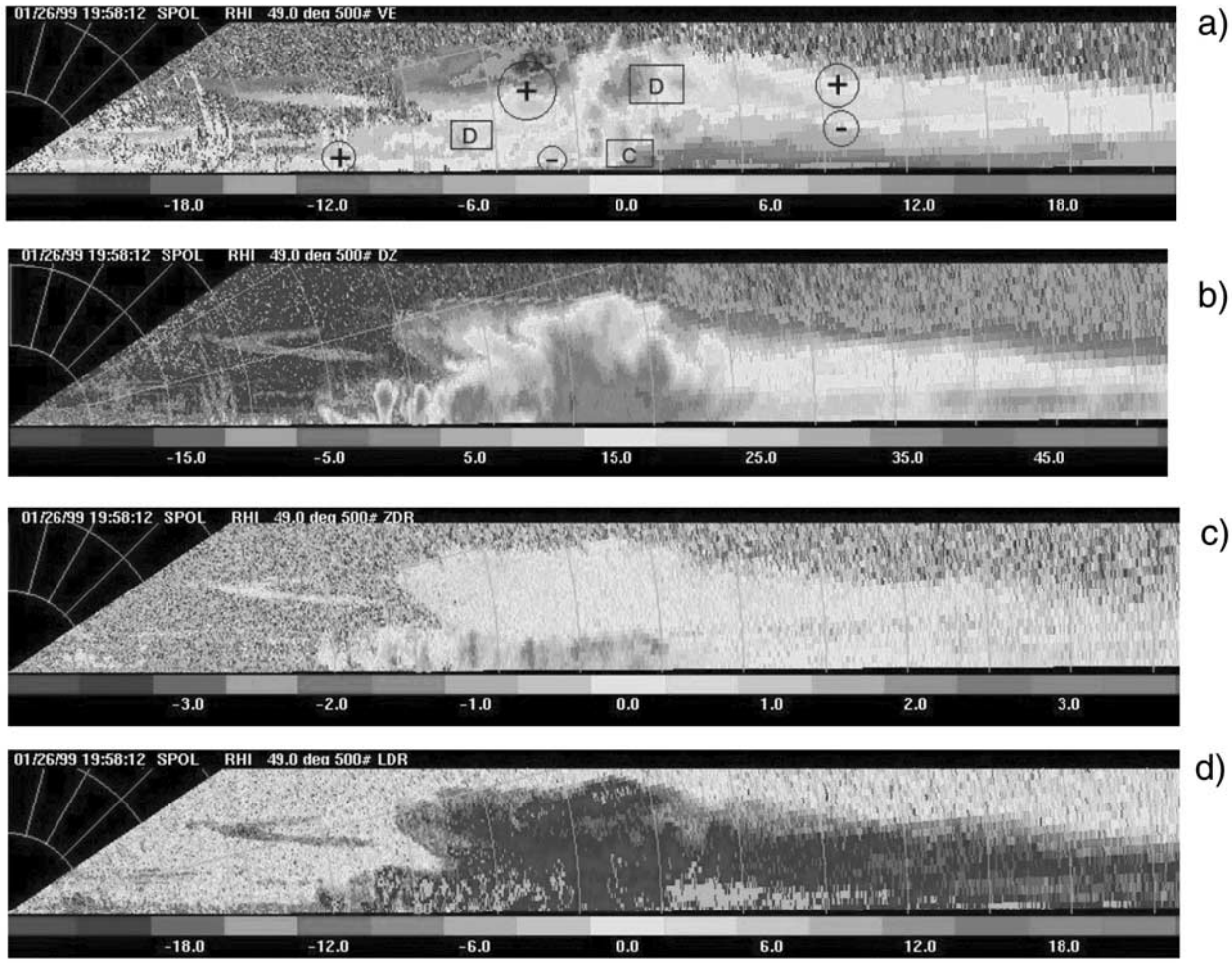

Figure 4. Vertical cross sections of radial wind (a), reflectivity (b), differential reflectivity (c), and linear polarization (d) at 49° measured with the S-POL weather radar at 1958 UTC, 26 January 1999 in Rondônia, Brazil. Colorscale at the bottom of each map are in m s^{-1} (a), dBZ (b), dB (c and d). Concentric circles indicate the distance from the radar at 10 km steps and straight lines indicate the elevations at 15° steps. Aspect ratio of horizontal and vertical scales 1:1. In the radial velocity field signs "+," "−," "c," and "d" indicate counterclockwise rotation, clockwise rotation, convergence, and divergence signatures, respectively.

region and due to coarse beam resolution in the stratiform region, but the zero isotherm is at 4.5 km height (Figure 5).

[15] Microphysical structures can be seen Figures 4c and 4d. The differential reflectivity cross section shows values between 0 and 2.5 dB everywhere in the precipitating system (Figure 4c). Several vertical bands of higher Z_{DR} below the melting layer are associated with larger drops. The most intense bands are at 57 and 64 km range ahead and outside the area of mature cells. In this particular area, reflectivities are higher while differential reflectivities are less positive, that is, there are considerably more drops of smaller diameter. The linear polarization cross section (Figure 4d) indicates negative values between −6.0 (aloft) to −21.0 dB everywhere in the system. Ice crystals aloft tend to form flat plates even though the environmental air temperature is below −30 °C above 450 hPa. The reflectivities above the freezing level are small for three main reasons: (1) ice crystals have much smaller refraction index (20%); (2) most of the moisture supplied by low-level convergence is consumed by warm cloud processes of diffusion, collision and coalescence; and (3) weak updrafts which do not loft much liquid water into the mixed phase region.

3.2. Radiosonde and Surface Measurements

[16] Upper level measurements in Rolim de Moura (Figure 1) are shown in Figure 5 for 1800 and 2100 UTC, 26 January 1999. During this time period, a maximum heating rate of 0.5 °C h^{-1} occurred between 400 and 600 hPa. The surface mixing ratio, almost constant up to 900 hPa, increased from 16 to 17 g kg^{-1}. The highest rate of increase was 0.9 g kg^{-1} h^{-1} in between 600 and 750 hPa. Since the humidity sensor used at the Rolim de Moura site has a dry bias [*Zipser and Johnson*, 1998; *Miloshevich et al.*, 2001], the mixing ratio estimates might be underestimated. Equivalent potential temperature profiles at 1800 UTC, 26 January 1999 and at 0000 UTC, 27 January 1999 (not

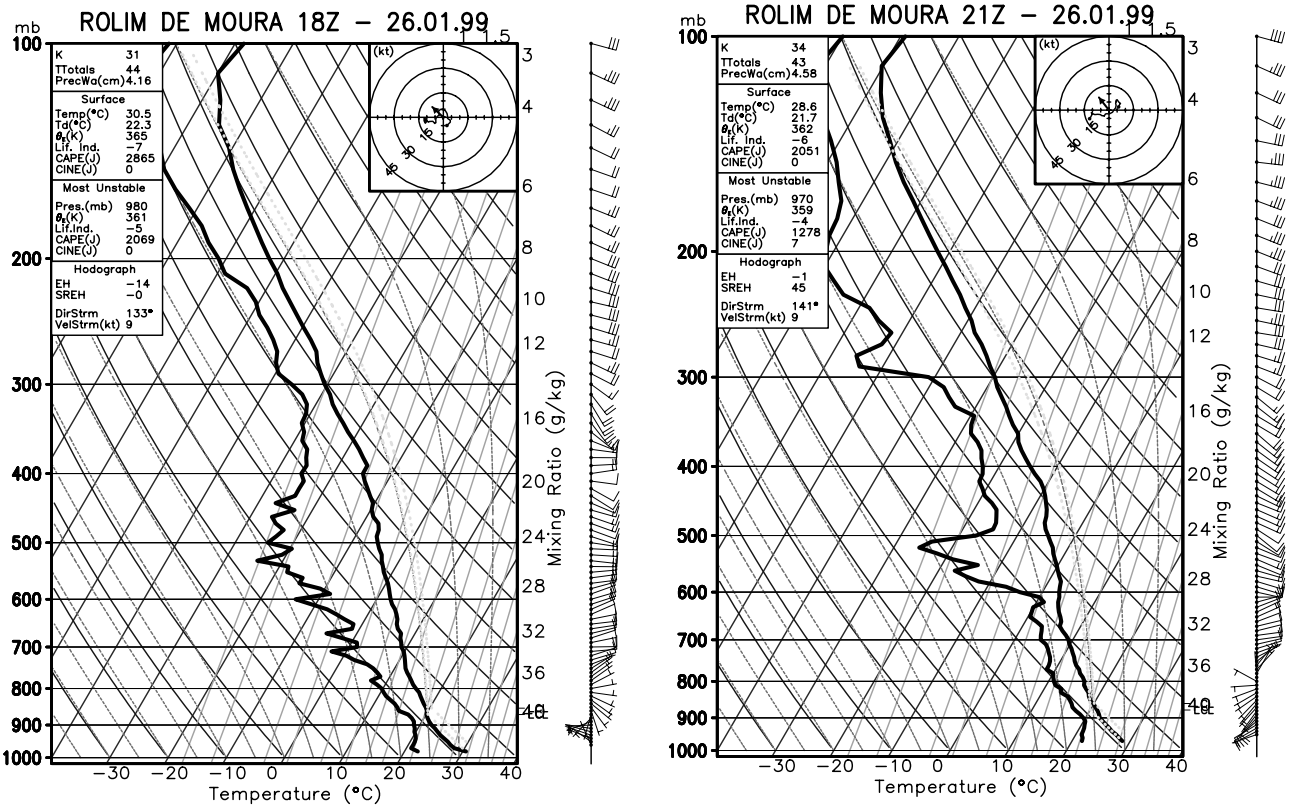

Figure 5. Vertical profiles of air temperature (°C), dew point temperature (°C), wind speed (m s^{-1}) and direction (°) at Rolim de Moura, Rondônia (Figure 1) for 26 January 1999 during the TRMM-LBA field experiment. Stability indexes are indicated.

shown) indicate an average cooling of 7 K below 820 hPa and average warming of 7 K between 820 and 300 hPa. On the other hand, the mixing ratio decreased by 3 g kg^{-1} below 820 hPa and increased by 2 g kg^{-1} between 820 and 300 hPa. The convective available potential energy (CAPE) of 2830 J kg^{-1} at 1800 UTC indicated strong convection and estimated maximum vertical velocity of 75 m s^{-1} [*Bluestein*, 1993], 3 hours before the passage of the squall line. However, water loading, perturbed vertical pressure gradients, and mixing effects reduce these estimates by 50% [*Weisman and Klemp*, 1986]. Preliminary wind retrieval results indicate maximum vertical velocities of 25 m s^{-1}. It did not rain before 2130 UTC in Rolim de Moura (Figure 6). The wind profiles did not change significantly above 700 hPa between 1800 and 2100 UTC (Figure 5). Below 700 hPa, the wind direction slightly backed with height at 1800 UTC while it gently veered with height at 2100 UTC which indicates some warm and cold advection, respectively.

[17] Surface measurements at Rolim de Moura (Figure 6) indicate that the squall line passed through the site around 2130 UTC. The surface pressure decreased significantly between 2115 and 2145 UTC due to the mesolow pressure center of 956.3 hPa. This large pressure drop might have resulted from strong subsidence caused by hydrostatic compensation especially ahead of the squall in the anvil region (Figure 4). This effect was measured in the wake low of a midlatitude squall line and was caused by the rear inflow jet [*Johnson*, 2001]. However, part of this large pressure drop was caused by dynamic pressure errors due an average wind gust of 8 m s^{-1}. The pressure chamber did not have a horizontal port to cancel dynamic effects. After 2100 UTC, the pressure tendency indicates the approaching mesohigh associated with convective region. The air temperature also decreased 9°C in a half hour. Equivalent potential temperature profiles (not shown) suggest that this colder air was brought down from 820 hPa.

[18] Winds from WNW changed to NE between 2130 and 2330 UTC with strong gusts during the transition of direction. This transition was caused by the gust front. The 15 min rainfall accumulation of 28 mm ending at 2215 UTC shows a time delay of 45 min between the passage of the gust front and the storm mature phase. This is consistent with radar measurements (Figure 4) which yield a time delay of 48 min considering the velocity of the cold pool (12 m s^{-1}) and the distance between the mature cells and young convective cells ahead of the squall line (35 km).

3.3. Vertical-Pointing Radar and Disdrometer Measurements

[19] Time-height cross sections of reflectivity, vertical wind and spectral width are shown in Figure 7 for the Ji-Paraná Airport site (Figure 1). These profiles show horizontal variations due to the movement of the system and temporal variations due to the system evolution. The reflectivity profile shows cloud tops higher than 10 km at 2100 UTC during the passage of the squall. The stratiform cloud tops are below 6 km and not well organized and persistent as measured by the S-POL radar (Figure 4) since it has a much

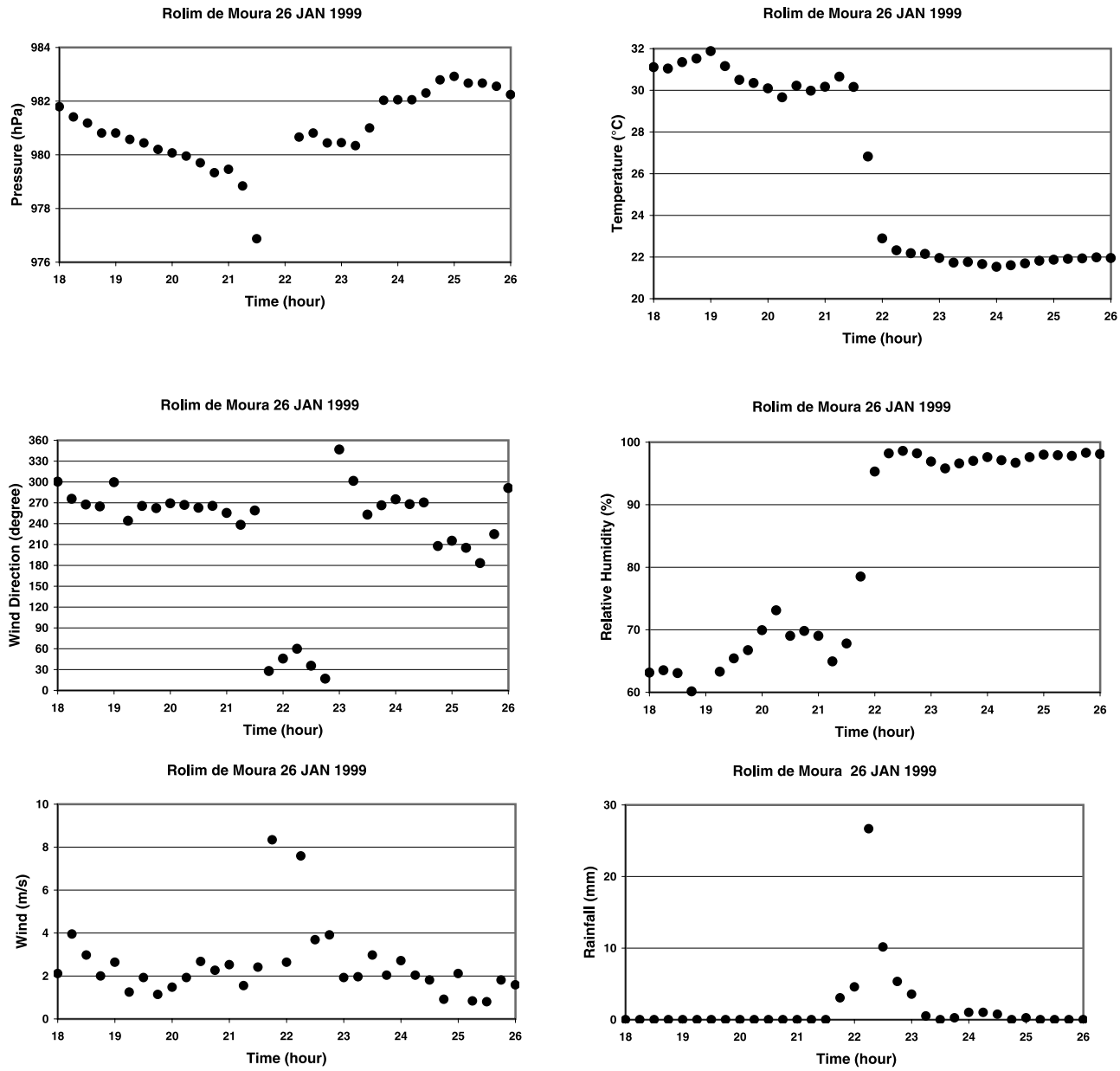

Figure 6. Time evolution of pressure, wind speed and direction, temperature, relative humidity, and rainfall accumulation as measured by the surface station in Rolim de Moura, Rondônia on 26 January 1999 during the TRMM-LBA experiment.

smaller sampling volume, but apparently the stratiform region was quickly shrinking with time (Figure 1). Initially, reflectivities increased rapidly between 3 and 6 km and were followed by high rainfall rates below 3 km. Higher reflectivities are observed between 2 and 7 km. The stratiform region associated with very low rainfall rates or none follows the convective region. The bright band can be easily identified in the stratiform area at 4.5 km around 2200 UTC. It is only 300 meters deep. This level is consistent with the 2100 UTC sounding where the zero isotherm is close to 650 hPa (Figure 5). Thus above this level one might expect to find ice crystal and snow. The reflectivities above and below are lower than at this level because of the melting of ice crystals and snow [*Fabry et al.*, 1995]. Above the melting layer, the reflectivities are small due to the lower ice refraction index. Below it, reflectivities become smaller due to an decrease in drop diameter.

[20] The bright band can also be seen in the Doppler velocity field. The phase change from ice or snow to liquid water increase the terminal velocity. For instance, at 2200 UTC, the terminal velocity above the melting layer is 2 m s^{-1} and below it 8 m s^{-1}. Fast terminal velocities in the cloud top region at 2045 UTC associated with ice crystals and snow (lower reflectivities) suggest that they are induced by strong subsidence in the anvil region (Figure 4). Furthermore, the spectral width shows strong turbulence aloft caused by the updrafts within the convective region and subsequent downdrafts by mass continuity. This strong subsidence can explain the great surface pressure fall by hydrostatic warm in Rolim the Moura at about 2130 (Figure 6).

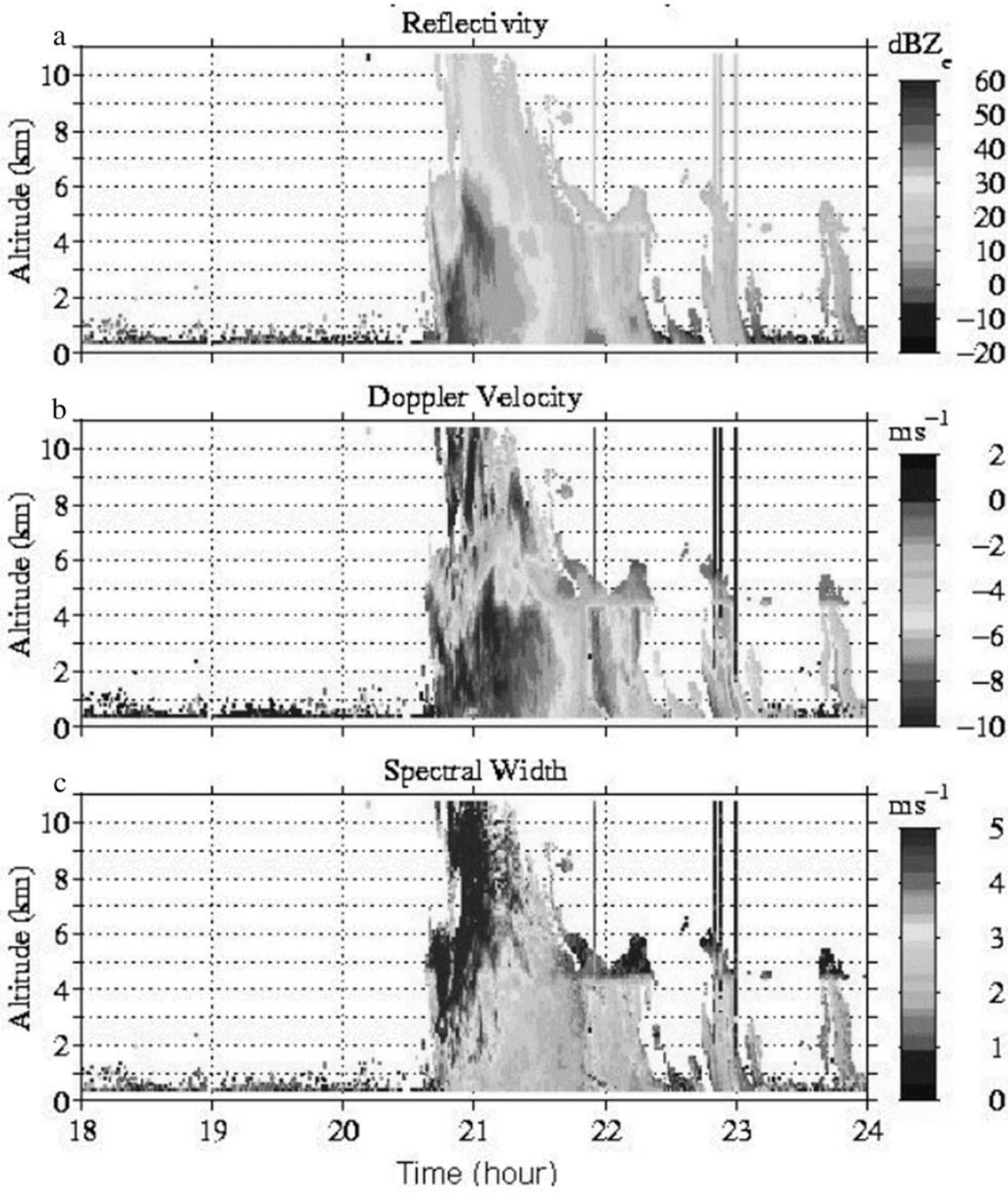

Figure 7. Time-height cross section of reflectivity (a), vertical velocity (b), and spectral width (c) measured with vertical-pointing radar at Ji-Paraná Airport, Rondônia on 26 January 1999 during the TRMM-LBA experiment. Colorscale indicates intensities.

[21] These reflectivity profiles are analyzed in conjunction with the drop-size spectrum measured at the Ji-Paraná Airport (Figure 8). Initially, the drop-size spectrum is composed of large drops that yield high reflectivities. As the spectrum shifts toward lower drop sizes with time it broadens keeping the reflectivity fairly constant. The drop-size spectrum is monomodal within the convective region between 2050 and 2100 UTC. The transition between convective to stratiform rainfall lasts less than 5 min. Within this short time period, the drop-size spectrum is bimodal.

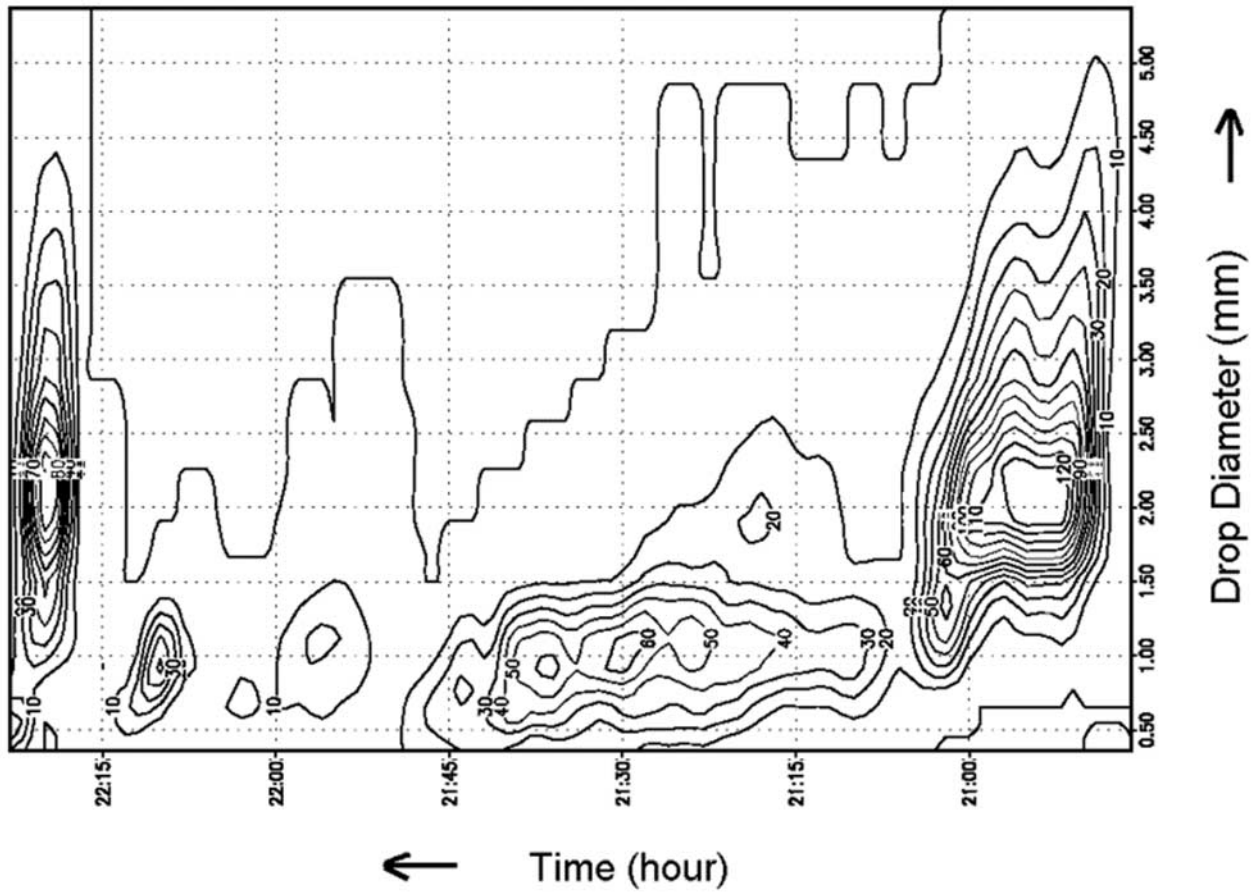

Figure 8. Temporal evolution of the drop-size spectrum measured at the Ji-Paraná Airport with a membrane disdrometer on 26 January 1999 during the TRMM-LBA field experiment. Contours indicate the number of drops of a given diameter.

After this transition, an almost constant monomodal spectrum is prevailing in the stratiform region with a dominant drop diameter around 1.0 mm.

[22] An inspection of both Figures 7 and 8 shows a striking similarity between surface reflectivities and the drop spectrum and also reveal the resulting microphysics associated with the squall line. The large drops are the first to fall through the updrafts. It is possible that the largest drops reach the surface first because of their terminal velocity and that evaporation in the initial stage of a shower eliminates the smallest droplets in the unsaturated air. Another possible explanation is the high droplet growth efficiency produced by turbulence in midlevels shown in Figure 7b between 2050 and 2100 UTC. Thus they probably reach midlevels at the most during this short time period (Figure 7a). As large amounts of water is removed by precipitating larger drops, less water vapor and liquid water is available, reducing the growth rate efficiency. Smaller droplets are carried further up where liquid water change to ice crystals as suggested in Figure 7a from 2100 to 2110 UTC. Eventually, these ice crystals and snow fall through the melting layer to produce stratiform rainfall from 2110 to 2215 UTC. A comparison of the S-POL radar measurements and disdrometer estimations of reflectivity over the Ji-Paraná Airport also indicate good agreement (Figure 9). Thus these various data sets are consistent with each other. The above drop spectra differ from the ones by *Tokay and Short* [1996] measured during the Tropical Ocean Global Atmosphere Couple Ocean-Atmosphere Experiment (TOGA COARE) since almost 80% of the convective and stratiform precipitation events were associated with very light to moderate rainfall.

[23] The convective region produced downdraft velocities of 10 m s^{-1} and thus midlevel colder air was dragged down to form the cold pool at the surface. This is consistent with the thermodynamic analysis for Rolim the Moura soundings. It also can be inferred that the warm microphysics is dominant in the convective region while cold microphysics is prevailing in the stratiform region. The cold pool is a result of midlevel air dragging by large drops in the mature phase of convection. Once the CAPE is released, strong updrafts carry boundary layer warm and moist air to midlevels where turbulence generated by eddies increase the efficiency of warm microphysics processes of diffusion, collision and coalescence.

4. Conclusions

[24] Results indicate several similarities between the analyzed equatorial squall line of 26 January 1999 and its cousins in midlatitude. However, the stratiform rainfall

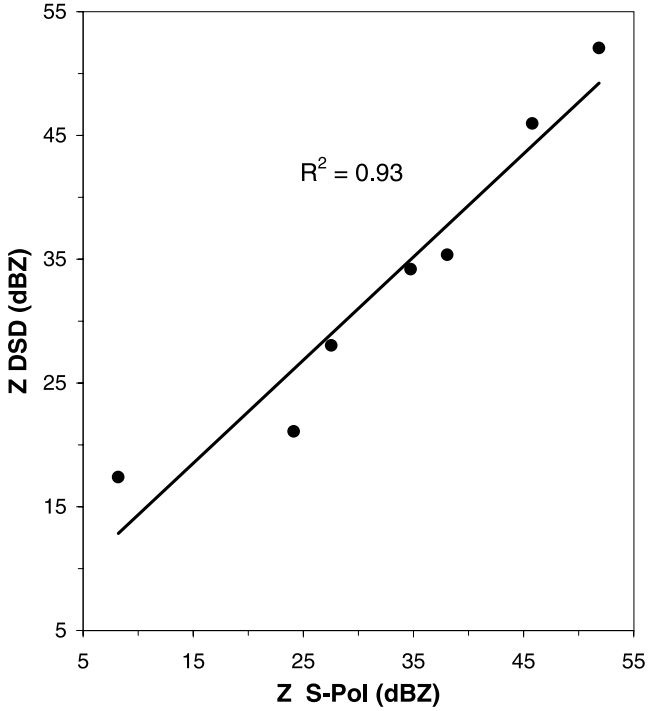

Figure 9. Scatter diagram of measured and estimated reflectivities by the S-POL radar and the disdrometer at the Ji-Paraná Airport, respectively. The data correspond to the squall line on 26 January 1999 during the TRMM-LBA field experiment. It is indicated the variance coefficient.

region, the transition zone and the mesoscale high are less remarkable then those analyzed by *Johnson and Hamilton* [1988] and *Smull and Houze* [1987]. On the other hand, a front-to-rear ascending flow and a rear descending flow are well defined by *Houze et al.* [1989]. Polarimetric measurements were helpful in identifying hydrometeor types within the squall line and their effect on maintaining this precipitating system [*Liu et al.*, 1997]. Significant changes in temperature, humidity and winds were observed below 850 hPa during the passage of the squall line. There was an increase in temperature throughout the troposphere with drying above and moistening below 600 hPa mainly caused by latent heat release. Surface and upper level data are consistent with radar measurements concerning the velocity of propagation of the squall line (12 m s^{-1}), rainfall rates and the bright band level (4.5 km).

[25] Radar data shows an ascending flow in the environment and descending flow at mid and low-level in the stratiform region. Strong updrafts are produced by low-level convergence resulting from the moving cold pool and the hydrostatic warming caused by divergence aloft and subsidence to compensate the updrafts. The cold pool air has its origin in midlevels where evaporative cooling and large drop-dragging generate strong downdrafts in the mature phase of the convective region. A rear low-level jet helps to balance horizontal circulation and to keep the tilted updrafts. These observations corroborate the conceptual model proposed by *Garstang et al.* [1994].

[26] Strong mid to upper level turbulence in the developing phase of convection caused by eddies increase cloud droplet growth and might explain the observed drop-size spectrum evolution. It is suggested that the convective region is dominated by warm microphysics while the stratiform region by cold microphysics. It is monomodal in the convective (2.0 mm) and stratiform (1.0 mm) regions, but bimodal in the transition. Vertical-pointing and S-POL reflectivity measurements agree very well with disdrometer reflectivity estimates. The melting layer is 300 m deep and more evident in the stratiform region, where significant changes in terminal velocity and reflectivity take place. The present study will contribute to modeling efforts of such system in the wet season of the Amazon region.

[27] **Acknowledgments.** The authors are thankful to all participants in the TRMM-LBA field experiment that directly or indirectly contributed to the success of the project. They also would like to thank three anonymous reviewers that greatly improved this work with their suggestions, comments and positive criticism. This research was sponsored by "Fundação de Amparo à Pesquisa do Estado de São Paulo" under grant 1997/09926-9. The leading author received partial support from the National Research Conceal CNPq under grant 300076/98-3.

References

Abdoulaev, S., and O. Lenskaia, Severe squall lines, I, Classification, paper presented at 9th Brazilian Meteorological Congress, Braz. Meteorol. Soc., Campos do Jordão, São Paulo, Brazil, 6–13 Nov., 1996a.

Abdoulaev, S., and O. Lenskaia, Severe squall lines, part 2, Causes and consequences of velocity variations, paper presented at 9th Brazilian Meteorological Congress, Braz. Meteorol. Soc., Campos do Jordão, São Paulo, Brazil, 6–13 Nov., 1996b.

Abdoulaev, S., and O. Lenskaia, Severe squall lines, part 3, Kinetic structure, paper presented at 9th Brazilian Meteorological Congress, Braz. Meteorol. Soc., Campos do Jordão, São Paulo, Brazil, 6–13 Nov., 1996c.

Ambrizzi, T., Numeric study of precipitating bands associated with trapezoidal instability, M.S. thesis, 74 pp., Inst. of Astron. and Geophys. of the Univ. of São Paulo, São Paulo, Brazil, 1989.

Beneti, C. A. A., Analysis of vertical integrated liquid water for nowcasting, M.S. thesis, 105 pp., Inst. of Astron. and Geophys. of the Univ. of São Paulo, São Paulo, Brazil, 1991.

Biggerstaff, M. I., and R. A. Houze Jr., Kinematic and precipitation structure of the 10–11 June 1985 squall line, *Mon. Weather Rev.*, *119*, 3034–3065, 1991a.

Biggerstaff, M. I., and R. A. Houze Jr., Midlevel vorticity structure of the 10–11 June 1985 squall line, *Mon. Weather Rev.*, *119*, 3066–3079, 1991b.

Bluestein, H. B., *Synoptic-Dynamic Meteorology in Midlatitudes*, vol. 2, *Observations and Theory of Weather Systems*, 594 pp., Oxford Univ. Press, New York, 1993.

Braun, S. A., and R. A. Houze Jr., The transition zone and secondary maximum of radar reflectivity behind a midlatitude squall line: Results retrieved from Doppler radar data, *J. Atmos. Sci.*, *51*, 2733–2755, 1994.

Browning, K. A., and F. H. Ludlam, Airflow in convective storms, *Q. J. R. Meteorol. Soc.*, *88*, 117–135, 1962.

Cohen, J. C. P., M. A. F. Silva Dias, and C. A. Nobre, Environmental conditions associated with Amazonian squall lines: A case study, *Mon. Weather Rev.*, *123*, 3163–3174, 1995.

Ecklund, W. L., C. R. Williams, P. E. Johnston, and K. S. Gage, A 3-GHz profiler for precipitating cloud systems, *J. Atmos. Oceanic Technol.*, *16*, 309–322, 1999.

Fabry, F., A. Bellon, and I. Zawadzki, Measurement of attenuation at X-band in the melting layer, paper presented at 27th Conference on Radar Meteorology, Am. Meteorol. Soc., Vail, Colo., 9–13 Oct., 1995.

Fovell, R. G., and Y. Ogura, Numerical simulation of a midlatitude squall line in two dimensions, *J. Atmos. Sci.*, *45*, 3179–3846, 1988.

Fovell, R. G., and Y. Ogura, Effect of vertical wind shear on numerically simulated multicell storm structure, *J. Atmos. Sci.*, *46*, 3144–3176, 1989.

Gandú, A. W., Statistical analysis of radar echoes associated with precipitating system in the east region of São Paulo State, M.S. thesis, 161 pp., Inst. of Astron. and Geophys. of the Univ. of São Paulo, São Paulo, Brazil, 1984.

Garreaud, R. D., and J. M. Wallace, The diurnal march of convective cloudiness over the Americas, *Mon. Weather Rev.*, *125*, 3157–3171, 1997.

Garreaud, R. D., and J. M. Wallace, Summertime incursions of midlatitude air into subtropical and tropical South America, *Mon. Weather Rev.*, *126*, 2713–2733, 1998.

Garstang, M., H. L. Massie Jr., J. Halverson, S. Greco, and J. Scala, Amazon coastal squall lines, part I, Structure and kinematics, *Mon. Weather Rev.*, *122*, 608–622, 1994.

Gash, J. H. C., C. A. Nobre, J. M. Roberts, and R. L. Victoria, *Amazonian Deforestation and Climate*, 611 pp., John Wiley, New York, 1996.

Gomes, A. M., M. A. Lima, and M. A. Antonio, Doppler characteristics associated to severe storms in the São Paulo State, paper presented at 9th Brazilian Meteorological Congress, São Paulo, Brazil, 1996.

Greco, S., J. Scala, J. Halverson, H. L. Massie Jr., W.-K. Tao, and M. Garstang, Amazon coastal squall lines, part II, Heat and moisture transports, *Mon. Weather Rev.*, *122*, 623–635, 1994.

Hastenrath, S., Annual cycle of upper air circulation and convective activity over the tropical Americas, *J. Geophys. Res.*, *102*, 4267–4274, 1997.

Houze, R. A., Jr., S. A. Rutledge, M. I. Biggerstaff, and B. F. Smull, Interpretation of Doppler weather radar displays of midlatitude mesoscale convective systems, *Bull. Am. Meteorol. Soc.*, *70*, 608–619, 1989.

Houze, R. A., Jr., B. F. Smull, and P. Dodge, Mesoscale organization of springtime rainstorms in Oklahoma, *Mon. Weather Rev.*, *118*, 613–654, 1990.

Johnson, R. H., Surface mesohighs and mesolows, *Bull. Am. Meteorol. Soc.*, *82*, 13–31, 2001.

Johnson, R. H., and P. J. Hamilton, The relationship of surface pressure features to precipitation and airflow structure on a intense midlatitude squall line, *Mon. Weather Rev.*, *116*, 1444–1472, 1988.

Lenskaia, O., and S. Abdoulaev, Severe squall lines, part VI, Surface impact, paper presented at 9th Brazilian Meteorological Congress, São Paulo, Brazil, 1996.

Lima, M. A., Mesoscale objective analysis: Observing network and characterization of organized precipitating systems, M.S. thesis, 166 pp., Inst. of Astron. and Geophys. of the Univ. of São Paulo, São Paulo, Brazil, 1985.

Liu, C., M. W. Moncrieff, and E. J. Zipser, Dynamical influence of microphysics in tropical squall lines: A numerical study, *Mon. Weather Rev.*, *125*, 2193–2210, 1997.

Lutz, J., P. Johnson, B. Lewis, E. Loew, M. Randall, and J. VanAndel, NCAR's S-Pol: Portable polarimetric S-band radar, paper presented at 9th Conference on Meteorological Observations and Instrumentation, Am. Meteorol. Soc., Charlotte, N. C., March 27–31, 1995.

Machado, L. A. T., R. L. Guedes, J. M. B. Silveira, R. C. Waltz, and M. A. S. Alves, Live cycle of convective systems, paper presented at 8th Brazilian Meteorological Congress, Braz. Meteorol. Soc., Belo Horizonte, Minas Gerais, Brazil, 18–25 Oct., 1994.

Miloshevich, L. M., H. Vömel, A. Paukkunen, A. J. Heymsfield, and S. J. Oltmans, Characterization and correction of relative humidity measurements from Vaisala RS-80-A radiosondes at cold temperatures, *J. Atmos. Oceanic Technol.*, *18*, 135–156, 2001.

Negri, A. J., E. N. Anagnostou, and R. F. Adler, A 10-yr climatology of Amazonian rainfall derived from passive microwave satellite observations, *J. Appl. Meteorol.*, *39*, 42–56, 2000.

Parker, D. J., Cold pools and shear, *Q. J. R. Meteorol. Soc.*, *122*, 1655–1674, 1996.

Pereira Filho, A. J., B. P. F. Braga Jr., M. T. L. Barros, and C. V. M. Carrera, Flood forecasting: Can weather radar help?, paper presented at 9th Brazilian Symposium on Water Resources, Braz. Assoc. of Water Resour., Rio de Janeiro, Brazil, 10–14 Nov., 1991.

Rotunno, R., J. B. Klemp, and M. L. Weisman, A theory for strong, long-lived squall lines, *J. Atmos. Sci.*, *45*, 463–485, 1988.

Scolar, J., Temporal evolution on synoptic conditions associated to prefrontal squall lines, M.S. thesis, 85 pp., Inst. of Astron. and Geophys. of the Univ. of São Paulo, São Paulo, Brazil, 1983.

Seitter, K. L., A numerical study of atmospheric density current motion including the effects of condensation, *J. Atmos. Sci.*, *43*, 3068–3076, 1986.

Silva Dias, M. F., Mesoscale meteorology, South American phenomena, and mesoscale forecasting and its applications—Lectures presented at the fortieth session of the WMO Executive Council, *WMO Rep. 712*, World Meteorol. Org., Geneva, 1989.

Silva Dias, M. A. F., Storms in Brazil, in *Routledge Hazards and Disasters Series*, vol. 2, *Storms*, edited by R. Pielke Sr. and R. Pielke Jr., pp. 207–219, Routledge, New York, 1999.

Silva Dias, M. A. F., Clouds and rain processes in a biosphere atmosphere interaction context in the Amazon Region, *J. Geophys. Res.*, *107*, 8072, 10.1029/2001JD000335, 2002.

Silva Dias, M. A. F., and R. N. Ferreira, Application of a linear spectral model to the study of Amazonian squall line during GTE/ABLE 2B, *J. Geophys. Res.*, *97*, 20,405–20,419, 1992.

Smull, B. F., and R. A. Houze Jr., Dual-Doppler radar analysis of a midlatitude squall line with trailing region of stratiform rain, *J. Atmos. Sci.*, *44*, 2128–2148, 1987.

Tokay, A., and D. Short, Evidence from tropical raindrop spectra of the origin of rain from stratiform versus convective clouds, *J. Appl. Meteorol.*, *35*, 355–371, 1996.

Tokay, A., O. W. Thiele, A. Kruger, and W. F. Krajewski, New measurements of drop-size distribution and its impact on radar rainfall retrievals, paper presented at 29th International Conference on Radar Meteorology, Am. Meteorol. Soc., Montreal, Que., Canada, July 12–16, 1999.

Weisman, M. L., and J. B. Klemp, Characteristics of isolated convective storms, in *Mesoscale Meteorology and Forecasting*, edited by P. S. Ray, pp. 331–358, Am. Meteorol. Soc., Boston, Mass., 1986.

Zipser, E. J., and R. H. Johnson, Systematic errors in radiosonde humidities: A global problem?, paper presented at 10th Symposium on Meteorological Observations and Instrumentation, Phoenix, Ariz., Jan. 11–16, 1998.

Zrnic, D. S., and A. V. Ryzhkov, Polarimetry for weather surveillance radars, *Bull. Am. Meteorol. Soc.*, *80*, 389–406, 1999.

R. I. Albrecht, A. W. Gandu, O. Massambani, A. J. Pereira Filho, and M. A. F. Silva Dias, Universidade de São Paulo, Rua do Matão 1226, São Paulo-SP 05508-9000, Brazil. (rachelif@model.iag.usp.br; adwgandu@model.iag.usp.br; omassamb@model.iag.usp.br; apereira@model.iag.usp.br; mafdsdia@model.iag.usp.br)

L. G. P. Pereira and S. Rutledge, Colorado State University, Fort Collins, CO 80523-1371, USA. (gustavo@atmos.colostate.edu; rutledge@radarmet.atmos.colostate.edu)

A. Tokay, NASA Goddard Space Flight Center, Code 912.1, Greenbelt, MD 20771, USA. (tokay@radar.gsfc.nasa.gov)